GA–A27404

FULLY GYROKINETIC MODELING OF BEAM-DRIVEN ALFVÉN EIGENMODES IN DIII-D USING GYRO

by
E.M. BASS and R.E. WALTZ

SEPTEMBER 2012

DISCLAIMER

GA–A27404

FULLY GYROKINETIC MODELING OF BEAM-DRIVEN ALFVEN EIGENMODES IN DIII-D USING GYRO

by
E.M. BASS* and R.E. WALTZ

This is a preprint of a paper to be presented at the Twenty-fourth IAEA Fusion Energy Conf., October 8-13, 2012 in San Diego, California.

*University of California San Diego, La Jolla, California.

Work supported by
the U.S. Department of Energy
under DE-FG02-95ER54309 and DE-FC02-08ER54977

GENERAL ATOMICS PROJECT 03726
SEPTEMBER 2012

Fully Gyrokinetic Modeling of Beam-Driven Alfvén Eigenmodes in DIII-D Using GYRO

E.M. Bass 1) and R.E. Waltz 2)

1) University of California, San Diego, 9500 Gilman Dr., La Jolla, CA 92093-0417, USA
2) General Atomics, PO Box 85608, San Diego, California 92186-5608, USA

e-mail: ebass@ucsd.edu

Abstract. The unstable spectrum of Alfvén eigenmodes (AEs) driven by neutral beam-sourced energetic particles (EPs) in a benchmark DIII-D discharge (142111) is calculated in a fully gyrokinetic model using the GYRO code's massively parallel linear eigenvalue solver. One cycle of the slow (equilibrium scale) frequency sweep of the reverse shear Alfvén eigenmode (RSAE) at toroidal mode number n=3 is mapped. The RSAE second radial harmonic and an unstable beta-induced Alfvén eigenmode (BAE) are simultaneously tracked alongside the primary RSAE. An observed twist in the eigenmode pattern is caused mostly by shear in the driving EP profile. Coupling to the BAE and to the toroidal Alfvén eigenmode limit the RSAE frequency sweep at the lower and upper end respectively. While the present fully gyrokinetic model (including thermal ions and electrons) constitutes the best treatment of compressibility physics available, the beta-induced BAE frequency is overpredicted by about 20% against experiment here and is found to be sensitive to energetic beam ion pressure. The RSAE frequency is more accurately matched except when it is limited by the BAE. Simulations suggest the experiment is very close to marginal AE stability at points of RSAE-BAE coupling.

1. Introduction

In fusion plasmas, a population of energetic particles (EPs) with a radial pressure gradient provides a source of free energy that can couple to high frequency instabilities through a variety of kinetic resonances. The Alfvén eigenmodes (AEs) are an important class of such instabilities likely to be driven by fusion-born alpha particles in ITER [1] and future fusion devices. Alpha confinement may be significantly degraded. A variety of AEs observed in modern fusion experiments (e.g., [2]) are usually driven unstable by energetic ions sourced from neutral beam injection (NBI) heating. In many cases, the unstable AEs are seen to induce substantial transport of these energetic beam ions.

Here, we examine the linear physics of unstable reverse shear Alfvén eigenmodes (RSAEs) [3], toroidal Alfvén eigenmodes (TAEs) [4], and beta-induced Alfvén eigenmodes (BAEs) [5] driven by NBI-sourced EPs in the benchmark DIII-D discharge 142111 [6–8] using the gyrokinetic continuum code GYRO [9,10]. This discharge features a minimum in the magnetic safety factor q, necessary for the existence of the RSAE. The DIII-D data show measurable beam profile flattening by RSAE and (to a lesser extent) TAE transport. The present linear study is restricted to the spectrum of AEs with toroidal mode number $n = 3$ around the discharge time $t = 725$ ms. The experimental spectrum is dominated by $3 \le n \le 5$. Encouraging agreement with experiment is achieved in the predicted mode frequency and eigenmode structure.

The RSAE stays on the $q = q_{\min}$ surface, where a flattening of the shear Alfvén wave dispersion produces a gap in the continuum. The mode propagates at the Alfvén speed v_A along the field line, giving rise to a slow (equilibrium time scale) upward and downward sweep of the RSAE frequency $\omega_{RSAE} \approx v_A \left| (nq_{\min} - m)/q_{\min} R \right|$ as the current ramps up. Here $q_{\min}$ is the minimum value of q, m is the poloidal mode number, and R is the torus

major radius. The RSAE frequency sweep is bounded by TAE coupling at the high end and BAE coupling at the low end [11].

The TAE stays between singular surfaces (which move with the current ramp up) in a toroidally-induced Alfvén continuum gap. The parallel wave vector is fixed giving a constant frequency $\omega_{TAE} \approx v_A/2qR$, where the safety factor $q = (m \pm 1/2)/n$ halfway between singular surfaces. The mode is composed of adjacent poloidal harmonics m and $m+1$.

The BAE is composed of one principle poloidal harmonic, peaking on the corresponding singular surface. Its frequency $\omega_{BAE} \approx (v_A/R)(\gamma\beta)^{1/2}$, where γ is the specific heat ratio and β is the ratio of thermal to magnetic pressure, lies at the top of a lower continuum gap induced by Alfvénic coupling to sound waves. Separation between this finite beta-induced gap and the reverse shear and toroidicity-induced gap becomes small when $q_{min} \approx m/n$, near the low points of the RSAE frequency sweep. Then the reverse-shear frequency gap, which would otherwise approach zero frequency, abuts the finite-beta gap and the RSAE down sweep is arrested at the BAE frequency. The present simulations see a strongly unstable BAE near these points of RSAE-BAE coupling. We will see below that the unstable BAE may be an artifact of unphysically strong EP drive in the simulation. The experimental spectrogram does not show an unstable BAE.

The GYRO model treats all species — thermal ions, electrons, and beam EPs — gyrokinetically (Ref. 9 for details). Recent simulation work [8,12] has demonstrated that, at a minimum, self-consistent inclusion of kinetic EPs is required to recreate the level of up-down symmetry breaking observed in experiments [6]. From the perspective of the present linear simulations, a kinetic treatment of thermal particles assures the most accurate prediction of kinetic damping, additional (probably minor) up-down symmetry breaking effects in the eigenmodes, and coupling to sound waves via parallel compressibility.

The present linear study uses GYRO's full gyrokinetic eigenvalue solver. This SLEPc-PETSc-based [13,14] solver finds the spectrum of leading eigenmodes using the full gyrokinetic phase space. While the solver was previously only applicable to small local simulations [15], an enhanced parallelization scheme now allows solutions of much larger problems such as the present global case. We will see below that four separate modes fight for dominance over the RSAE frequency sweep examined, and that the eigenvalue solver illuminates the influence of subdominant modes in the RSAE frequency cascade.

2. Simulation Parameters

All simulations presented here center around the t =725 ms time of reverse-shear, beam heated DIII-D discharge 142111. The domain covers the plasma core region defined by $0.15 \le \rho \le 0.80$, where $\rho \equiv \sqrt{\chi_t/\chi_{t0}}$ and χ_t is the toroidal flux having value χ_{t0} at the last closed flux surface. An up-down symmetric Miller [16,17] equilibrium is used in the simulation and maps extremely well to experimental flux surface geometry for this minimally shaped case.

The shear-reversed safety factor q profile is shown in Fig. 1(a). In the present study, we adjust the minimum safety q_{min} by applying a uniform multiplicative factor over the whole q profile. The thermal particle and beam ion temperature and density profiles are shown in Fig. 1(b,c). The thermal temperatures T_i and T_e are obtained directly from experimental

diagnostics as is the electron density n_e. The MHD equilibrium fit gives the total pressure P_{MHD}. The effective temperature T_{EP} of the artificially Maxwellian beam is chosen to match the second velocity moment (proportional to pressure) to that of the classical beam deposition profile. We cannot use the classical result for the density because the active Alfvén eigenmodes studied here cause substantial EP transport and flatten the core of the distribution. Instead, the remaining two variables n_{EP} and n_i are given by the pressure relationship $P_{MHD} = n_e T_e + n_i T_i + n_{EP} T_{EP}$ and the assumption of quasi-neutrality $n_e = n_i + n_{EP}$ (impurities are neglected in this study).

The low rotation of this discharge (around 2.6 kHz at the q_{min} surface), including a Doppler shift of about 8 kHz for n=3 modes on the q_{min} surface, is neglected in the calculations. The experimental $E \times B$ shearing rate at the q_{min} surface $\gamma_E \equiv (\rho/q)(\partial\omega_0/\partial\rho)\big|_{q=q_{min}} \geq 0.6$ kHz is well below observed linear growth rates and unlikely to produce a strong change in the linear eigenmodes. Here ω_0 is the toroidal fluid rotation frequency.

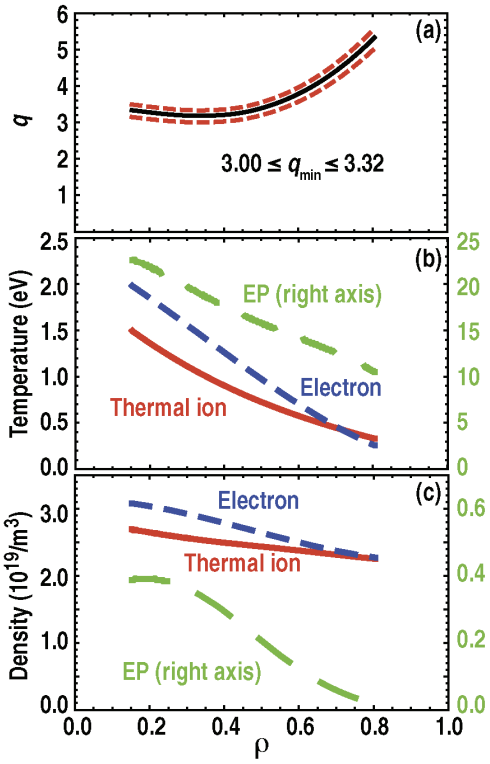

FIG. 1. Equilibrium profiles of DIII-D discharge 142111 used in the simulations. The q profile (a) is adjusted with a uniform multiplier to scan q_{min}. The three species temperatures (b) and densities (c) represent the best match to experimental values under the charge neutrality constraint.

Unless otherwise stated, all results reported come from GYRO's recently implemented gyrokinetic global eigenvalue solver. GYRO is fully electromagnetic with $[\delta\phi, \delta A_\parallel, \delta B_\parallel]$ perturbations, however, for the present EP stability study, $\delta B_\parallel$ is suppressed and ∇B is set to curvature per the low-k MHD rule [17]. The magnetic compressibility $\delta B_\parallel$ has been found to have negligible impact in selected test cases. Collisions are neglected. The grid dimensions for each of the three kinetic species (ion, electron, and EP) are as follows: 300 radial (flux surface), 20 poloidal (different grids for passing and trapped particles), 8 pitch angle (4 passing and 4 trapped), and 8 energy (extending to six times the relevant species' local temperature). The GYRO toroidal grid is spectral, and we limit our linear investigation here to n=3. The (dense) matrix in the associated eigenvalue problem has 1,152,000 rows and columns. While much more computationally intensive than an initial-value calculation, the eigenvalue solver allows calculation of a spectrum of modes for each set of input parameters.

The eigenvalue solver often returns spurious high frequency solutions with unphysically large growth rates, sometimes in excess of the leading growth rate. These and other low-k_r modes are inherently damped by GYRO's hybrid explicit-implicit Eulerian time step and consequently do not appear in initial-value calculations. The high-frequency eigenvalue solver solutions have been determined to be unphysical artifacts and are consequently discarded. Reported results include the remaining solutions.

3. Mode Properties

At least three distinct unstable Alfvén eigenmodes are identified at each choice of parameters. Modes are categorized primarily based on the eigenfunction structure, shown in Fig. 2 for electrostatic potential ϕ at q_{min}=3.28. In the adiabatic approximation, fluctuations in ϕ are proportional to electron temperature fluctuations. The poloidal cross-sections [Fig. 2(a-c)] and harmonic decompositions [Fig. 2(d-f)] reveal features typical of RSAEs, TAEs, and BAEs, sometimes in the same mode. At the chosen value of q_{min}=3.28, the leading mode [Fig. 2(a,d)] is consistent with a BAE. The main peak lies on the q=10/3 surface, well off q_{min}, and is dominated by the m=10 poloidal harmonic [Fig. 2(d)]. The mode tail is more TAE-like, consisting at each point of two main (albeit kinetically broadened) poloidal harmonics. No precise formula for the kinetic BAE frequency exists, but it should be just below the RSAE frequency for the chosen value of q_{min}=3.28. The first subdominant mode is the primary RSAE [Fig. 2(b,e)]. It sits on the q_{min} surface and is dominated by one poloidal harmonic (m=10). A third mode [Figs. 2(c,f)] has a TAE-like main peak extended to high ρ and RSAE-like secondary peaks (one poloidal component m=10) near the q_{min} surface. The q_{min}-centered peaks can be identified with the RSAE second radial harmonic. The two RSAE frequencies lie just above the dominant BAE frequency, further supporting that mode's identification as a BAE. Note that the RSAE and TAE can only be considered as distinct modes away from the overlap condition $q_{min}\approx(m+1/2)/n$. In general, the three unstable modes identified here are best characterized as a linearly interacting, kinetic AE trio as q_{min} evolves.

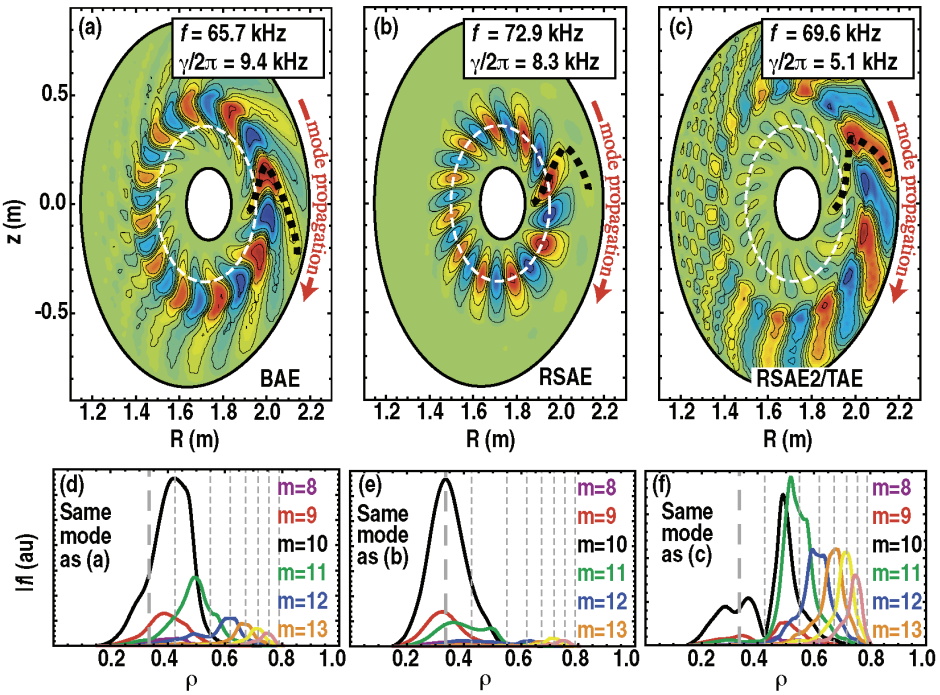

FIG. 2. Electrostatic potential ϕ contours (a-c) and poloidal harmonics of |ϕ| (d-f) for the three leading modes at q_{min}=3.28. The leading mode (a) is the BAE. The two subdominant modes are the RSAE (b) and the RSAE second harmonic hybridized with a TAE (c). The mode propagates in the ion diamagnetic direction (red arrows), meaning the open end of the mode arrowhead pattern (emphasized with black dashed curves) leads, not the point.

The twisted pattern in the eigenfunction structures indicated by the dashed black curves in Fig. 2(a-c) is a universal feature in the present simulations. Similar patterns have been observed in experiments [6], but are precluded in up-down symmetric ideal MHD, i.e. marginally driven ideal MHD EP modes have no twist. Other kinetic codes, including GTC [18], TAEFL [19], and M3D-K [20] have reproduced similar twists in the eigenfunction structure [8], but some disagreement exists on the precise pattern. Comparisons between the various models represented by these codes suggest self-consistent EP kinetic physics as the primary source of the twisting. All modes propagate clockwise [for the right-side images shown in Fig. 2(d-f)], in the ion diamagnetic direction. The open end of the apparent "arrowhead" pattern [(emphasized by the dashed black curves in Fig. 2(a-c)], not the point, leads. This feature manifests in all modes in the present study and is a common feature in experiment as well [8,21].

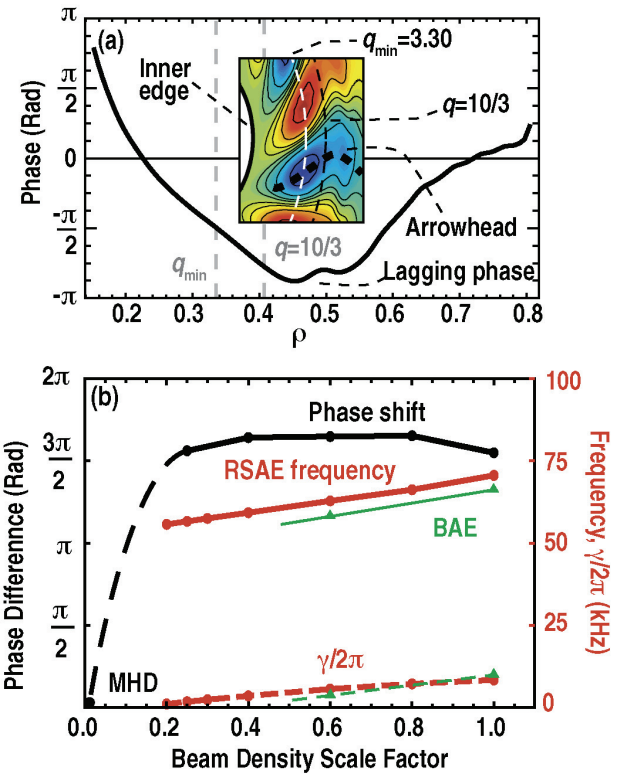

FIG. 3. Phase progression across flux surfaces. The phase vs ρ at the outboard midplane at experimental beam density (a) shows a lagging phase near q=10/3 (ρ=0.41) which gives rise to arrowhead patterns such as those in Fig. 2(a-c), here shown for the (subdominant) RSAE at q_{min}=3.30 (inset). Phase shift from the inner boundary (ρ=0.15) to q=10/3 (b) varies little with beam drive strength (mode is dominant for $n_{EP} \leq 0.8 n_{EXP}$). RSAE frequency and growth rate are shown in red, with select BAE values shown in green for Ref. 3.

The shearing pattern comes from a phase shift in the eigenfunction envelope across flux surfaces. Figure 3(a) shows the ϕ eigenfunction complex phase on the outboard midplane as a function of ρ for the RSAE at q_{min}=3.30. The turnover in phase gives rise to the arrowhead shape seen in a poloidal section [black dashed curves in Fig. 2(a-c) and Fig. 3(a), inset]. We quantify the degree of twisting as the phase difference along the outboard-midplane path between the inner simulation domain boundary (ρ=0.15) and the first singular surface (q=10/3 at ρ=0.41) outside the q_{min} surface, chosen as a convenient fixed marker near the empirical phase turnaround point. We see in Fig. 3(b) that cross-surface phase shift changes little as EP drive is reduced to the marginal point. The tracked RSAE is the dominant mode at all points shown except at $n_{EP}=n_{EXP}$, where it is the first subdominant mode. Accordingly, the initial-value solver is used for RSAE data points with $n_{EP}<n_{EXP}$. While reducing drive does effectively eliminate the high-ρ mode tail, the interior mode shearing remains nearly constant. If peaking in the driving EP density gradient $-\partial n_{EP}/\partial r$ caused the observed shearing, the expected phase shift projected to $n_{EP}=0$ would be zero contrary to Fig. 3(b). For a variety of physical and numerical reasons stable modes are difficult to find, precluding points for

stable values of n_{EP} in Fig. 3(b). The implied steep descent of the curve in Fig. 3(b) in the AE stable region of n_{EP}<0.2(dashed black curve) reflects a poorly understood subtlety of the process by which EPs induce the cross-surface phase shift. However, the weak scaling of phase shift with n_{EP} in Fig. 3(b) is consistent with the variation of (or shear in) the EP diamagnetic drift velocity ($\propto -\partial \ln n_{EP}/\partial r$), which is independent of the size of n_{EP}, as the principle phase shift-inducing asymmetry. RSAE frequency and growth rate are shown in red in Fig. 3(b) with select BAE values from the eigenvalue solver shown in green for reference.

As q_{min} decreases with the current ramp up, it sweeps through the TAE-RSAE overlap condition. Figure 4 shows the frequency and growth rate of four salient n=3 Alfvén eigenmodes tracked by the gyrokinetic eigenvalue solver over the sweep range $3.32 \geq q_{min} \geq 3.00$, a complete cycle from m=10 to m=9 dominance. Modes are color coded and connected to preclude frequency crossing of unstable AEs. The black curve shows the characteristic RSAE frequency up-sweep most prominently. The RSAE second harmonic (blue curve) is subdominant in the up-sweep phase, but dominant in the down-sweep (q_{min}> 9.5/3). The experimental sweep, adapted from a beam emission spectroscopy (BES) spectrogram [6] and likely corresponding to these two modes, is shown in orange. The approximate upward Doppler shift of about 8kHz is subtracted from the experimental points for comparison with the rotation-free simulation. Initial-value solver results, shown in gray in Fig. 4(a,b), track the largest growth rate mode predicted by the eigenvalue solver as expected. The purple dots are unstable AEs not easily connected to the other modes.

The constant-frequency green curve, labeled BAE in Fig. 4(a,b), defines a lower bound on the frequency of other modes through linear mode-mode interaction, as expected for the RSAE-BAE pair. The mode has a consistently BAE-like (one main poloidal harmonic) peak on the inside, with TAE-like (two poloidal harmonics) tail peaks. The BAE-like peak grows well above the others at the high-q_{min} left side of the sweep in Fig. 4(a,b), as seen in the poloidal decomposition of Fig. 2(d). No direct evidence of the unstable BAE is found in experimental diagnostics, but the BES spectrogram does show a gap in the RSAE frequency cascade at a lower frequency that is probably related. The BAE frequency and growth rate are likely both over-predicted in the simulation.

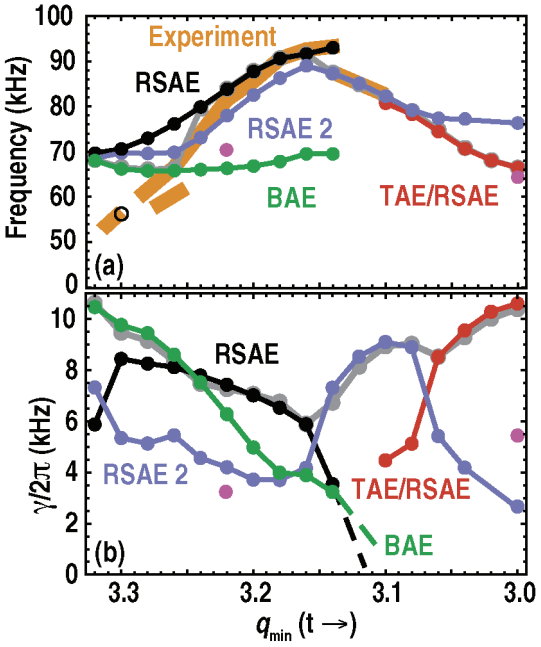

FIG. 4. The spectrum of frequency and growth rates for unstable Alfvén eigenmodes q_{min} as decreases in time. The frequency (a) shows characteristic RSAE up and down sweep (black, blue, red dots) as well as a fixed BAE frequency (green dots). Experimental BES values (orange lines) show RSAE and RSAE second harmonic frequencies reduced by 8 kHz to account for Doppler shift. The growth rates (b) illustrate that all modes compete for dominance over the scan. Initial-value solutions (gray dots) follow the dominant mode. Dashed growth-rate curves show projected decline to stable values. Purple dots show unstable AE eigenvalue solutions not easily connected to the other modes.

The increase of the RSAE frequency with n_{EP} shown in Fig. 3(b) (solid red curve) reflects the increase of the BAE "floor" frequency [green curve in Fig. 4(a) and solid green curve in Fig. 3(b)] with total plasma pressure. Between the marginal stability point and the experimental n_{EP} value, the RSAE frequency difference is about 15 kHz. This difference is the same as the difference between the GYRO RSAE frequency prediction and the measured value at the high q_{min}, early-time left side of Fig. 4(a), where interaction with the BAE is strong. Lowering n_{EP} diminishes the BAE frequency and growth rate, reducing it to subdominant status quickly by n_{EP}/ n_{EXP}=0.8. The BAE frequency floor is dropped, allowing the RSAE frequency to sweep to the lower value [open, black circle in Fig. 4(a)]. Both a reduction in the RSAE frequency and the removal of the unstable BAE bring the prediction more in line with the experimental spectrogram, suggesting that the beam density profile used here (assumed constant in time) may be overestimated for some time values. A gap in the experimental spectrogram suggests that the RSAE/BAE is stable near q_{min}=3.30 [Fig. 4(a), orange lines], and the RSAE frequency prediction near marginal stability [Fig. 3(b), reproduced as open circle in Fig. 4(a)] of 56 kHz agrees extremely well with experiment. No similar frequency variation with n_{EP} is seen near the center of the sweep range, where the upsweep is TAE limited rather than BAE limited. Determining the true value of marginal n_{EP} likely requires model refinements such as a more physical (non-Maxwellian) velocity distribution and regenerating self-consistent equilibria as total pressure is reduced.

5. Conclusions

A thorough examination of one RSAE frequency sweep in the benchmark DIII-D discharge 142111 by the gyrokinetic continuum code GYRO shows many points of agreement with the experiment. Qualitative details of eigenmode structure agree with experimental observations, and simulations recreate MHD-predicted interactions of the RSAE with the TAE at the overlap condition $q_{min}=(m+1/2)/n$ and with the BAE near $q=m/n$. These mode-mode couplings limit the RSAE frequency sweep at the upper and lower ends respectively. The RSAE frequency agrees with experiment within about 20% near the BAE-limited lower sweep range and within 2%–3% at the TAE-limited upper end. The BAE frequency, determined by total pressure, is somewhat over-predicted here, likely due to an overestimation of EP density. The GYRO global eigenvalue solver explicitly reveals all such linear mode couplings, including a clear demonstration that the RSAE down sweep connects directly to the up-sweeping RSAE second harmonic, not the principle RSAE (Fig. 4(a)).

GYRO predicts the twist in the eigenmode pattern seen by other codes that include self-consistent EPs. Both experimental and GYRO eigenfunctions are almost universally characterized by a region of lagging phase, giving rise to an arrowhead shape in the eigenfunction peak where the open end, not the point, leads as the mode propagates in the ion diamagnetic direction [Fig. 2(a-c)]. Radial phase variation is likely caused primarily by shear in the EP diamagnetic drift in the experiment.

Agreement with experimental frequencies is found to improve to within a few percent when the driving beam density is reduced below the experimental estimate, reducing the lower bound frequency and dropping the limiting BAE to subdominant or even stable status. This agreement is consistent with an apparent gap in the experimental spectrogram that

indicates diminished drive in this range. Sensitivity of frequency predictions to drive strength highlights the importance of accurate determination of the driving distribution for quantitative comparisons. To this end, a more accurate velocity-space dependence than the Maxwellian approximation used here may be called for in future work.

This work is funded by the US DOE SciDAC Gyrokinetic Simulation of Energetic Particles Turbulence and Transport (GSEP) under DE-FC02-08ER54977. Computational work was carried out at the Oak Ridge Leadership Computing Facility (OLCF) and the National Energy Research Scientific Computing Center (NERSC). The authors wish to thank M.A. Van Zeeland, B.J. Tobias, W.W. Heidbrink, G.-Y. Fu, and the entire GSEP team for valuable insights and feedback.

References

[1] GORELENKOV, N.N., BERK, H.L. BUDNY, R., CHENG, C.Z., FU, G.-Y., HEIDBRINK, W.W., KRAMER, G.J., MEADE, D., and NAZIKIAN, R., Nucl. Fusion **43** (2003) 594.
[2] VAN ZEELAND, M.A., KRAMER, G.J., NAZIKIAN, R, BERK, H.L., CARLSTROM, T.N., and SOLOMON, W.M., Plasma Phys. Controlled Fusion **47** (2005) L31.
[3] BERK, H.L., BORBA, D.N., BREIZMAN, B.N., PINCHES, S.D., SHARAPOV, S.E., Phys. Rev. Lett. **87** (2001) 185002.
[4] CHENG, C.Z., CHEN, Liu, and CHANCE, M.S., Ann. Physics **161** (1985) 21.
[5] TURNBULL, A.D., STRAIT, E.J. HEIDBRINK, W.W., CHU, M.S., DUONG, H.H., GREENE, J.M., LAO, L.L., TAYLOR, T.S., and THOMPSON, S.J., Phys. Fluids **B 5** (1993) 2546.
[6] TOBIAS, B.J., CLASSEN, I.G.J., DOMIER, C.W., HEIDBRINK, W.W., LUHMANN, Jr, N.C., NAZIKIAN, R., PARK, H.K., SPONG, D.A., and VAN ZEELAND, M.A., Phys. Rev. Lett. **106** (2011) 075003.
[7] TOBIAS, B.J., BOIVIN, R.L., BOOM, J.E., CLASSEN, I.G.J., DOMIER, C.W., DONNÉ, A.J.H., HEIDBRINK, W.W., LUHMANN, C., MUNSAT, T., MUSCATELLO, C.M., NAZIKIAN, R., PARK, H.K., SPONG, D.A., TURNBULL, A.D., VAN ZEELAND, M.A., YUN, G.S., and the DIII-D TEAM, Phys. Plasmas **18** (2011) 056107.
[8] SPONG, D.A., BASS, E.M., DENG, W., HEIDBRINK, W.W., LIN, Z., TOBIAS, B.J., VAN ZEELAND, M.A., AUSTIN, M.E., DOMIER, C.W., LUHMANN, Jr, N.C., Phys. Plasmas 19 (2012) 082511.
[9] CANDY, J. and WALTZ, R.E., J. Comput. Phys. **186** (2003) 545.
[10] CANDY, J. and WALTZ, R.E., Phys. Rev. Lett. **91** (2003) 045001.
[11] KRAMER, G.J., GORELENKOV, N.N., NAZIKIAN, R., and CHENG, C.Z., Plasma Phys. Controlled Fusion **46** (2004) L23.
[12] DENG, W., LIN, Z., HOLDOD, I., WANG, Z., XIAO, Y., and ZHANG, H., Nucl. Fusion **52** (2012) 043006.
[13] HERNANDEZ, V., ROMAN, J., and VIDAL, V., ACM Trans. Math. Softw. **31** (2005) 351.
[14] BALAY, S., BROWN, J., BUSCHELMAN, K., GROPP. W.D., KAUSHIK, D., KNEPLEY, M.G., CURFMAN McINNES, L., SMITH, B.F., and ZHANG, H., PETSc web page, http://www. mcs. anl. gov/petsc, 2011.
[15] BASS, E.M., and WALTZ, R.E., Phys. Plasmas **17** (2010) 112319.
[16] MILLER, R.L., CHU, M.S., GREENE, J.M., LIN-LIU, Y.R., and WALTZ, R.E., Phys. Plasmas **5** (1998) 973.
[17] WALTZ, R.E. and MILLER, R.L., Phys. Plasmas **6** (1999) 4265.
[18] LIN, Z., HAHM, T.S., LEE, W.W., TANG, W.M., and WHITE, R.B., Turbulent Transport Reduction by Zonal Flows: Massively Parallel Simulations, Science **281** (1998) 1835.
[19] SPONG, D.A., CARRERAS, B.A., and HEDRICK, C.L., Phys. Fluids **B 4** (1992) 3316.
[20] PARK, W., BELOVA, E.V., FU, G.Y., TANG, X.Z., STRAUSS, H.R., and SUGIYAMA, L.E., Phys. Plasmas **6** (1999)1796 (1999).
[21] TOBIAS, B.J., Private communication, January 2012.